Edinburgh Research Explorer

Effect of surface tension, viscosity, pore geometry and pore contact angle on effective pore throat

Effect of surface tension, viscosity, pore geometry and pore contact angle on effective pore throat

Cong Chao[1], Guangwen Xu[2], Xianfeng Fan[1*]

[1]Institute for Materials and Processes, School of Engineering, The University of Edinburgh, Edinburgh EH9 3JL, UK

[2]Institute of Industrial Chemistry and Energy Technology, Shenyang University of Chemical Technology

Abstract

Through experimental measurement and theoretical calculation, we have investigated the effect of surface tension, liquid viscosity and the capillary geometry (capillary gradient and tip diameter) on the effective pore throat, and the impact of the effective pore throat on pore resistance to two-phase interfaces formed from fluids with different viscosities and surface tensions. When a two-phase interface flows in channels with varied pore size, capillary force is insignificant in the section of the channel with an inner pore size greater than the effective pore throat, and the pressure drops in this section depend on capillary tip diameter, rather than the surface tension. Capillary force takes significant effect on the interface only when the pore size in a tapered capillary is smaller than the effective pore throat. Effective pore throat depends on fluid surface tension and the capillary geometry, but not on liquid viscosity. The higher the fluid surface tension, the larger the diameter of the effective pore

* Corresponding author: Tel.: +441316505678; Fax: +441316506551; Email: x.fan@ed.ac.uk

throat. A channel with a large tip diameter or gradient will give a large effective pore throat diameter. Fluid viscosity only affects the magnitude of the resistant pressure drops of fluid flows in constricted capillaries, but does not affect the effective pore throat diameter. The effective pore throat and the pressure profile measured in this study can be explained by the pore contact angle, but cannot be explained by the contact angle on a flat surface of the same materials.

Key words: Capillary resistance, Two-phase flows, Pore throat, Surface tension, Constricted capillary, Pore contact angle

Introduction

Immiscible two-phase flows in porous materials are involved in many technological, geophysical and biological processes [1], such as the movement of air and water in soils and rocks [2], the recovery of hydrocarbons from reservoirs, fluid transport in the gas diffusion layer of fuel cells [3, 4], micro reactors [5] and electronic chips [6], and microbubble-aided drug delivery [7, 8]. Resistance to two-phase flows has been commonly used to characterize the efficiency of transport processes, and is estimated by the pressure drop across a porous material. The flow resistance is governed by pore morphology, pore size and its throat [9, 10]), pore surface wettability [11, 12], and fluid properties (e.g. viscosity and surface tension[13, 14]), etc.

. Numerous researchers have investigated the impact of fluid properties [13, 14, 16], pore geometry [16-20] and operational conditions [21] on the resistance to single or two-phase flows in porous media. In 1982, Wardlaw demonstrated that the oil trapping is a function of contact angle and pore geometry (pore-to-throat ratio, pore diameter, and throat length, etc.)[15]. Many single and two-phase flows experiments have been conducted in slowly or abruptly constricted capillaries which are designed to mimic a single pore-throat structure [20, 34-37]. Liang et al. demonstrated that the total resistant pressure for a liquid drop passing through an abruptly constricted capillary is dependent on the pore to throat ratio, inclination angle, contact angle, and throat diameter[20]. However, to author's best knowledge,   some important aspects are still not clear. For example, what pore size can be seen as a throat based on hydrodynamic resistance has not been clearly defined, i.e. at which point a significant resistance occurs to two-phase flows in a channel with varied pore size. Moreover, if the pore throat is defined based on hydrodynamics, what factors will affect the pore throat. Will the pore throat be affected by the fluid properties and pore body?

Commonly, pore throats are regarded as the section or point with a minimal cross-sectional area in a flow path [22-24]. It can be evaluated directly through tomographic methods, e.g. micro-X-ray imaging and magnetic resonance imaging (MRI) [25-29]. The tomographic methods coupled with mercury injection porosimetry can estimate the size of pore throat in reservoir or aquifer

rocks, in which pressure difference measured across a core sample and the volume of mercury that intrudes into the sample material are employed to evaluate the distribution of pore volume and pore size [27, 30]. The data from mercury injection porosimetry is useful to describe the permeability of porous materials in a macroscopic sense, but is not helpful for understanding the impact of the geometry of individual pore on the resistance to fluids, which is particularly important in improving the efficiency of processes and treatments for micro reactors, electronic chips and microbubble-aided drug delivery. In pore-scale network modeling, the pore volume is simplified as two elements-pores and throats [32]. The throat length is roughly defined by subtracting the two pore lengths (different from the pore diameter) from the total length between two pores [28, 33]. However, the definition of a throat is somewhat arbitrary as pointed out by Blunt, and may affect the accuracy of prediction in multiphase flows modelling. Understanding the points at which fluids start to suffer from the resistance due to the constriction of the flow channel geometry will help to segment the pores and throats concisely.

The resistance of a pore throat to a two-phase flow is different from a single phase flow due to the capillary effect induced by the two-phase interface [38]. When two-phase flows in capillaries, the presence of air bubble results in an increase in the resistance, and the pressure increase phenomenon is the well-known 'Jamin' effect. Many researchers also reported an increase in pressure when oil drop-water flows in channels with varied diameters [34, 35, 39]. For

example, Cobos et.al [35] analyzed the emulsion flow with oil drops in a glass capillary with a diameter of 200 μm (tube) and 50 μm (throat), and a sudden increase in the pressure drop was observed when oil drops flow into the tapered section of a glass capillary. The sudden increase in the resistance has been simply seen as the effect of the capillary pressure and the difference in fluids viscosity. The mechanism for this increase remains to be clarified, such as where exactly the increase occurs, and what factors affect the sudden increase in the pressure drop. In low-permeability reservoirs, the 'Jamin effect' becomes severe with the progress of liquid displacement, and the resistance required to displace the oil phase from the reservoirs is significantly high due to the great pore size variations and pore-pore throat ratios [25, 40]. A clearer understanding of pore throat based on hydraulic resistance will help to reveal the mechanism of sudden increase in the resistant pressure, and the impact of pore geometry on pore resistance to fluid flows [41].

In this study, constricted capillaries were employed to understand the pore resistance to fluid flows, and the factors affecting the effective pore throat. The effective pore throat was defined firstly based on the pressure-drop profiles of two-phase flows in constricted capillaries. The effect of surface tension on the effective pore throat and pressure drop was studied through adjusting the fluid surface tension. Silicone oils with similar surface tensions, but a large difference in viscosities, were employed to investigate the effect of fluid

viscosity on the effective pore throat. It is the first time to use pore contact angle in the pressure drop calculation.

Theory

Hydraulic resistance to two-phase flows in a microchannel is mainly determined by capillary force, viscous/frictional force, buoyancy force, and fluid gravity. Weber number, Bond number and Capillary number given in equations (1), (2) and (3), have been used to evaluate the relative effect of inertial force, gravity forces and viscous force versus surface tension on a two-phase flow, respectively.

$$We = \frac{\rho r u^2}{\gamma} \tag{1}$$

$$Bo = \frac{(\rho_w - \rho_{nw})g l^2}{\gamma} \tag{2}$$

$$Ca = \frac{\mu u}{\gamma} \tag{3}$$

where ρ_w is the fluid density of wetting phase, ρ_{nw} is the fluid density of non-wetting phase, r is the radius of microchannels, u is superficial velocity of fluid, γ is liquid-vapor interfacial tension, g is gravitational constant, l is the characteristic length and μ is the dynamic viscosity of fluids.

As reported in literature, a thin liquid film exists uniformly between the microchannel inner surface and the gas phase when a long bubble of a fluid with negligible viscosity moves slowly and steadily in a microchannel filled with liquid. The liquid film is stagnant, and does not cause frictional pressure loss [42, 43]. The film thickness is proportional to *Ca* number ($\frac{d}{D} = 0.67 Ca^{2/3}$, where

D is the channel diameter) [44], which is negligible in this study due to the small magnitude of the Ca number as given in Table 1. Thus the effective channel diameter for fluids flow can be seen as the capillary diameter.

We and Bo number are much less than 1 (as shown in Table 1), therefore the inertial effects and gravity force can be ignored. Capillary effect is included when the Ca number is smaller than 10^{-5}. As the contraction of capillary geometry is not abrupt, the pressure drop resulting from the contraction is negligible. Gravity force and buoyancy force can be ignored as the capillary setup is maintained in a horizontal configuration. Therefore, the total pressure drop for two-phase flows in a constricted capillary is the sum of the capillary pressure drop and frictional pressure drop.

Table 1. Range of the experimental parameters in this study

u	2.36×10^{-5}- 0.0212 m/s	Bo	1.41×10^{-3}-0.0353
Ca	2.79×10^{-7}- 8.81×10^{-3}	We	1.1×10^{-8}- 3.57×10^{-4}
Re	1.41×10^{-5} - 2.3		

2.1 Young-Laplace equation

Young-Laplace equation has been commonly used to predict the capillary pressure difference across the bubble in a cylindrical capillary [11, 45-48]. It is expressed as the function of the surface tension and contact angle of the fluids, which is the Young-Laplace equation, given by,

$$P_c = P_n - P_w = \frac{2\gamma cos\theta}{r} \tag{4}$$

where r is the microchannel radius, and θ is the contact angle between a vapour-liquid interface and the channel inner surface.

2.2 Frictional pressure drop

The frictional pressure drop in fully developed laminar flow is calculated by Darcy-Weisbach equation,

$$\Delta P_f = f \frac{\Delta L \rho u^2}{2D} \tag{5}$$

where L is the channel length, u is the mean superficial velocity of the fluid, D is the channel diameter, and f is the Darcy friction factor.

For laminar flow, f is obtained through conventional equation (6),

$$f = \frac{64}{Re} \tag{6}$$

where Reynolds number is given by $Re = \frac{\rho u D}{\mu}$.

As the capillary diameter used in this study is not constant, the correlations for frictional pressure drop presented in literature are not suitable for tapered capillaries. We derived a new equation according to Darcy-Weisbach equation to predict the frictional pressure drop for fluids flow in tapered capillaries (the detailed derivation is described in reference [38]), given as:

$$\Delta P_f = \frac{f \rho Q^2}{\pi^2 k r^4} = 32 \frac{\mu Q}{\pi k r^3} \tag{7}$$

where k is the capillary gradient, defined as $k = (r_{et} - r_{tip})/L$, in which r_{et} is the radius of the effective pore throat, r_{tip} is the radius of the capillary tip, and L

is the distance between the effective pore throat point and the capillary tip (as shown in Fig.1).

2.3 Experimental capillary pressure drop

The experimental capillary pressure is obtained through subtracting the frictional pressure drop from the overall pressure drop measured. For single-phase flows (case 1 of Fig. 1), the overall pressure drop is given by,

$$\Delta P_{single} = \Delta P_{f1} + \Delta P_{f2} \tag{8}$$

where ΔP_{f1} is the frictional pressure drop of liquid in the tube with a bore size of 3 mm, ΔP_{f2} is the frictional pressure drop of liquid in the tapered section.
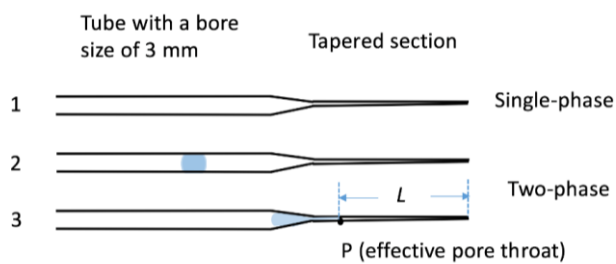

Fig. 1 A sketch of gas-liquid flows in a constricted capillary (bubble is shown in blue and liquid phase is shown in white)

For two-phase flows, when interface flows into the tapered section (case 3 of Fig. 1), the overall pressure drop ΔP_T is given by,

$$\Delta P_T = \Delta P_{f1} + \Delta P'_{f2} + \Delta P_c + \Delta P_{fg2} \tag{9}$$

Where $\Delta P'_{f2}$ is the frictional pressure drop of liquid in the tapered section (difference with ΔP_{f2} as the length occupied by liquid is changed), ΔP_{fg2} is the frictional pressure of gas phase in the tapered section and ΔP_c is the capillary pressure drop across the liquid-air interface in the tapered section.

Capillary pressure across the interface, ΔP_c can be obtained through equation (8) and (9),

$$\Delta P_c = \left(\Delta P_T - \Delta P_{single}\right) + \left(\Delta P_{f2} - \Delta P'_{f2} - \Delta P_{fg2}\right) \tag{10}$$

ΔP_T and ΔP_{single} were obtained experimentally through recording the overall pressure drop for two-phase and single-phase flows, respectively. Other terms, the frictional pressure drop for liquid phase and gas phase in constricted capillary (ΔP_{f2}, $\Delta P'_{f2}$ and ΔP_{fg2}) were calculated by equation (7).

Materials and methods

3.1 Manufacture of constricted capillaries

Constricted capillaries with different inner diameters and gradients were manufactured from borosilicate glass tubes with an inner diameter of 3 mm; (FB51467 Fisher Scientific, UK). To avoid any contamination, the glass tubes were soaked in 5M sodium hydroxide solution for 30 minutes (Fisher Scientific) and rinsed thoroughly with deionized water (C540 Deionizer, Veolia Water Solutions Technologies). The glass tube was then soaked in acetone for another 30 minutes (Fisher Scientific, A/0600/15), and washed with deionized water again. The glass tubes were then heated to around 550 °C by a D2-BS

0617 butane to remove any organic contaminant. After cooling, the tube is ready for manufacturing constricted capillaries with suitable tip sizes. The length of the capillary constricted section was controlled at around 3.5 cm and the pore size gradually decreases at a constant gradient and the tip has the smallest pore size. Two subsections of the constricted section (as shown in Fig. 1) were manufactured to achieve significant decrease of the channel diameter from 3000 μm to below 300 μm, and to investigate pore size effect in a large range. The experimental setup shown in Fig. 2 contains a liquid pump (LC-20 AD, Shimadzu), a pressure transducer with 0.01 mbar resolution, and a long working distance microscope with a long working distance (Brunel Microscope Ltd, 10x objective) fitted with a digital camera (AM7023 Dino-Eye, Dino-Lite Digital Microscope).

3.2 Measurement of pressure drops for fluids flow in constricted capillaries

A gas-liquid interface was introduced through injecting 0.1 ml gas into the constricted capillary which was initially filled with DI water. Then, the pump with a controlled flow rate of 0.01 ml/min was operated for both single and two-phase flows in all experiments. The interface position is identified through marking the tapered section of capillary with intervals. The pressure drop was displayed on the pressure transducer and recorded every 0.25 second through a LabView software.
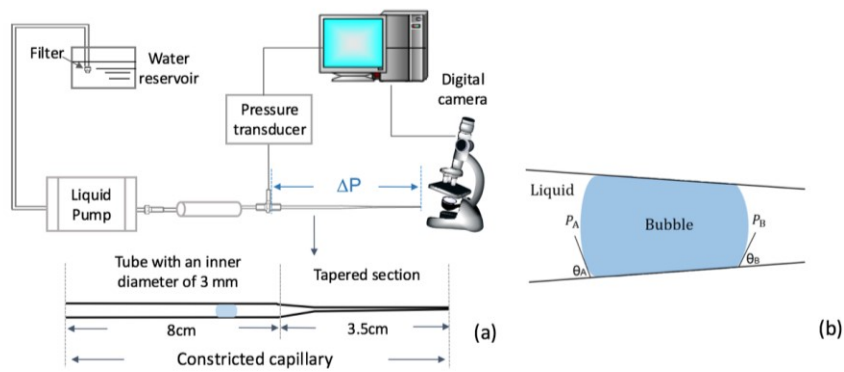
Fig. 2 Schematic of (a) the experimental apparatus and the tapered capillary (the tapered section consists of two subsections, and the tip diameter of the first subsection is about 1000 μm), and (b) a top view of a bubble in a constricted section of capillary in its static state

3.3 The effect of gas type on the effective pore throat

As CO_2 (C40-VB, BOC, Manchester), CH_4 (CP Grad (100%), BOC, Surrey) and air are the gases commonly used in fuel cells, gas reservoir and microbubble-aided drug delivery, respectively. Experiments in this section were designed to investigate the resistance of a constricted capillary to the interface created by these gases. The properties of these gases are shown in Table 2. During experiments, 0.1 ml of gas was injected respectively to create gas-water flows in constricted capillaries. The fluid flowrate was controlled at 0.01 ml/min and the pressure drop was recorded correspondingly.

Table 2. Physical properties of air, CO_2 and CH_4 (at 25°C and atmospheric pressure)

Gas	Density (kg/m^3)	Surface tension in water system (mN/m)
air	1.18	71.99
CO_2	1.98	72.0 [49]
CH_4	0.66	75.5 [50, 51]

3.4 The effect of surface tension on effective pore throat

To investigate the impact of liquid surface tension on effective pore throat and the fluid resistance, 2-propanol (99+ %, extra pure, ACROS Organics, New Jersey, U.S.A) and its aqueous solutions (with various mass fraction) were used as the liquid phase, and the air was the gas phase. As shown in Table 3, these solutions have a good contrast in surface tension. Their surface tension ranges from 21.22 mN/m for pure 2-propanol to 72.0 mN/m for DI water. Their viscosities were very close, ranging from $8.94×10^{-4}$ Pa·s (for DI water) to $2.07×10^{-3}$ Pa·s (for 2-propanol), and thus the difference in viscosity among these solutions can be ignored.

Table 3. Physical properties of aqueous solutions of 2-propanol and DI water (at 25°C and atmospheric pressure) [52, 53]

Concentration (w/w %)	Density (kg/m^3)	Viscosity (Pa·s)	Surface tension (mN/m)

0 (DI water)	997.05	8.94×10^{-4}	71.99
5	974.12	1.725×10^{-3}	49.58
20	913.17	3.040×10^{-3}	30.57
100	718.11	2.070×10^{-3}	21.22

3.5 The effect of liquid viscosity on effective pore throat

Silicone oils (sourced from MAPLLC Petroleum Crude Oil) were used as their viscosity varies greatly (as shown in Table 4) while their surface tension is similar, ranging from 20.1 to 21.2 mN/m. During the experiments, 0.1 ml silicone oil with different viscosity was injected to the constricted capillary which was initially filled with DI water to create immiscible oil-water flow, and the pressure drop profiles were recorded.

Table. 4 Physical properties of silicone oils [54-56]

| Silicone oil	Density (kg/m^3)	Viscosity $(Pa{\cdot}s)$	Surface tension (mN/m)	Interfacial tension against water (mN/m)
10cst	930	9.3×10^{-3}	19.4	43.4
50cst	960	4.8×10^{-2}	20.8	41.2
100cst	960	9.6×10^{-2}	20.9	41.0
500cst	970	4.85×10^{-1}	21.1	40.5

Results and discussions

4.1 Effective pore throat and resistant pressure profiles of two-phase flow in constricted capillaries

Effective pore throat of the constricted capillaries has been proposed and defined by our group based on the measured pressure drop profiles [38]. Fig. 3 presents a typical example to illustrate the definition of the effective pore throat (P Point in Fig. 3a), i.e. the pore size at which the resistant pressure suddenly increases. When the channel pore size is smaller than effective pore throat diameter, the capillary force to gas-liquid flows starts to be significant. This critical effective pore throat has been observed from our several hundred measurements. Fig. 4 presents additional typical pressure drop profiles for gas-liquids with different interfacial tension in constricted capillaries with different tip diameters. Some oscillation can be observed in the pressure profiles measured from tapered capillaries with larger tip diameter (as shown in Fig. 4a). The main reason is the magnitude of pressure drop in tapered capillaries with larger tip diameter is very small. In addition, the fluid surface tension, tip geometry of the tapered capillary affects the magnitude of fluctuation.
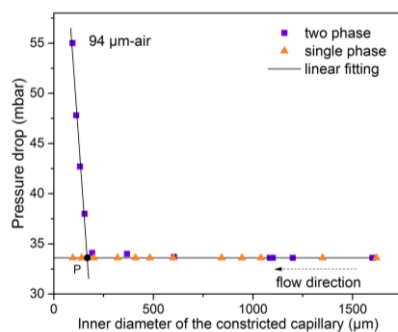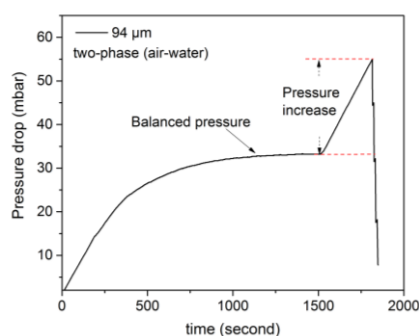
(a)   (b)

Fig. 3 (a) Method to evaluate the diameter of the effective pore throat (P Point), (b) pressure profile of an air-water flow in a constricted capillary with a tip diameter of 94 µm

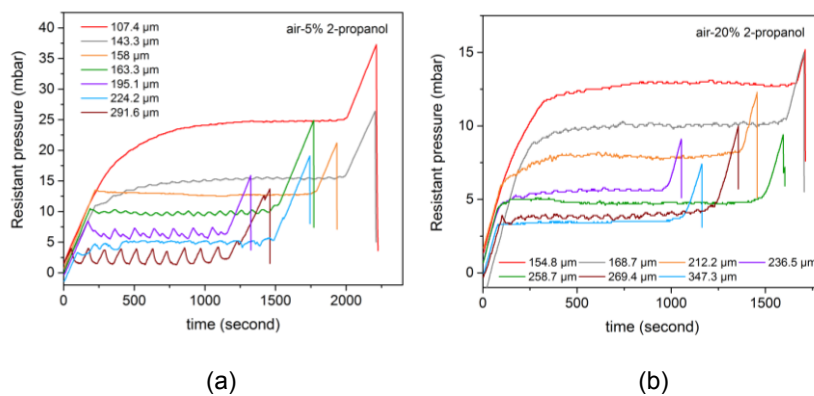(a)   (b)

Fig. 4 Resistant pressure profiles of (a) the air-5% 2-propanol flows and (b) the air-20% 2-propanol flows

The pressure increase in gas-liquid pressure profile is attributed to the capillary pressure induced by the gas-water interface when the pore diameter is smaller than the effective pore throat. 'Jamin' effect describes that the presence of air bubble retards the liquid flow in a tube with a small diameter, but does not indicate at which pore size the pressure increase happens in tortuous channels, and when the capillary force to the gas-liquid flow starts to be significant [35, 57-59]. Young-Laplace equation has been commonly employed to predict capillary pressure, and shows that the capillary pressure smoothly changes with the channel radius ($\Delta P_c \propto 1/r$), but also does not show at which pore size

the capillary force starts to be significant. The effective pore throat defined in this study clarifies this problem and indicates the pore size at which sudden increase starts and the capillary force takes effect.

4.2 Impact of gas phase on the effective pore throat

In this section, the effect of different gases on the effective pore throat and the resistance to gas-liquid flows in constricted capillaries have been investigated. Air, CO_2 and CH_4 were chosen as these gases are very common in fuel cells, electronic devices, CO_2 storage, shale gas recovery and microbubble-aided drug delivery. The typical experimental data have been presented in Figs 5-8. All of the data show that capillary resistance to the interfaces starts from the effective pore throat. Under the same capillary tip diameter, a larger surface tension of gas-water interface suffers a higher resistance. The effective pore throat diameter is very similar for three types of gas-water flows due to the similar surface tensions of three gases (as shown in Figs. 7 and 8).
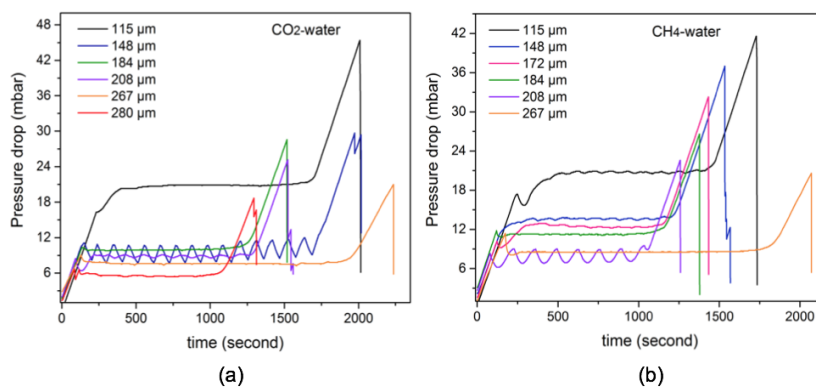

(a)   (b)

Fig. 5 Pressure-drop profiles for (a) CO_2-water and (b) CH_4–water flows in constricted capillaries with tip diameters in the range from 115 to 280 μm

The pressure profiles for three gas-water flows are very similar (Fig. 6), with a slight difference in magnitudes of pressure drop. For example, in the constricted capillary with a tip diameter of 116.8 μm (Fig. 6a), the CH_4-water interface has the highest pressure increase after the effective pore throat due to the greatest surface tension of CH_4-water (75.5 mN/m), while the air-water interface gives the lowest increase (lowest surface tension of air-water, 71.99 mN/m). Before the gas-water interface moves towards the effective pore throat, the pressure drop for the three type of gas-water flows is almost the same, as shown by the overlapping horizontal lines in Fig. 6.
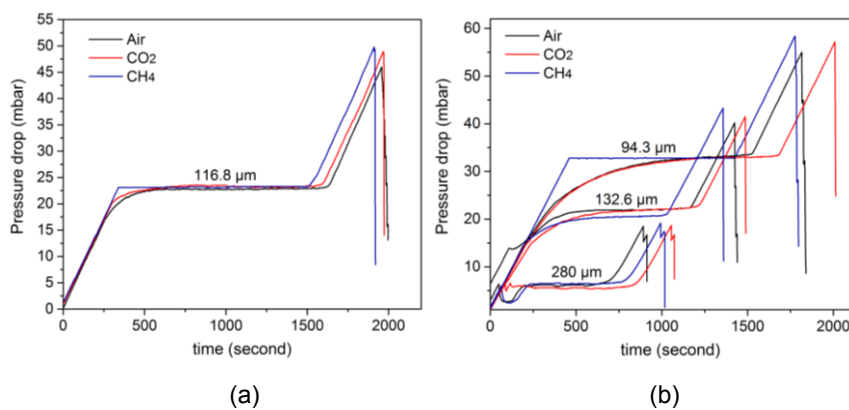

(a)   (b)

Fig. 6 Pressure drop profiles of air-water, CO_2-water, CH_4-water flows in the capillary with (a) the tip diameter of 116.8 μm, and (b) the tip diameter of 94.3, 132.6 and 280 μm
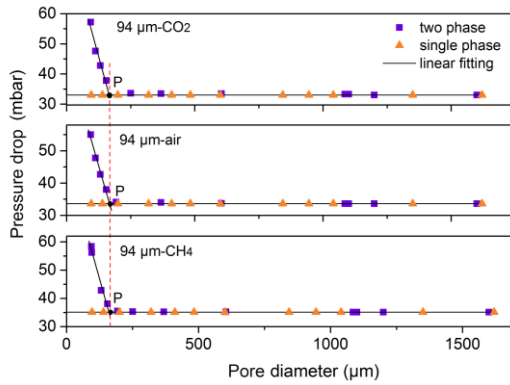
Fig. 7 Effective pore throat for air-water, CO_2-water, CH_4-water flows in the constricted capillary with a tip diameter of 94 μm
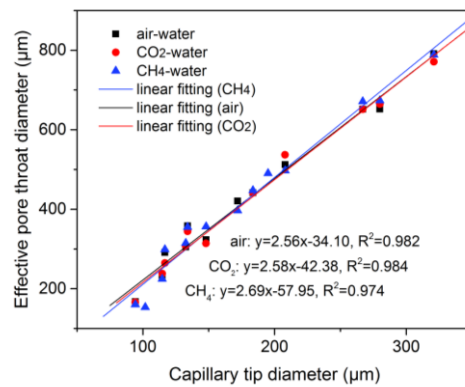

Fig. 8 Effective pore throat of the constricted capillaries for air-water, CO_2-water and CH_4-water flows

4.3 Impact of liquid surface tension on effective pore throat

To further investigate the impact of surface tension on the effective pore throat, 2-proponal was used to adjust the liquid surface tension from 71.99 to 30.57 mN/m. The physical properties of the liquids are shown in Table 3. The results

(Figs.9-10) indicate that the effect of surface tension on the pressure drop for two-phase flows takes action only after the effective pore throat, and a larger surface tension gives a larger resistance in constricted capillaries. For the flow path with a pore size greater than the effective pore throat, liquid surface tension does not affect the pressure drop of the flows, and the pressure drop is mainly controlled by the capillary tip size, rather than the surface tension. Small capillary tip gives a high resistance to two-phase flows. Moreover, the diameter of the effective pore throat increases with the increase of interface surface tension under the same flow conditions (flowrate, liquid viscosities) and capillary tip size, as shown in Fig. 10.

Fig. 9 (a) (b) and (c) show the pressure-drop profiles for the flows of air-water, air-5%wt 2-propanol and air-20%wt 2-propanol in constricted capillaries. In Fig. 9(a), the horizontal lines are the balanced pressure for two-phase flows before the interfaces touch the effective pore throat. The balanced pressure for air-water, air-5%wt 2-propanol and air-20%wt 2-propanol were about 6.1, 7.2, and 10.1 mbar, respectively. Although the surface tension of air-20%wt 2-propanol is the lowest (30.57 mN/m), the balanced pressure to air-20%wt 2-propanol flow is the highest as the capillary tip diameter is the smallest (218.6 μm). The surface tension of air-water is the highest but the balanced pressure is the lowest because of the relatively large capillary tip diameter (224 μm). This indicates that when the pore size of microchannel is greater than the effective pore throat, the resistant pressure drop is directly dependent on the capillary

tip sizes, rather than the surface tension. Fig. 9 (b) and (c) further prove the

dominant effect of capillary tip size on the resistant pressure before the effective
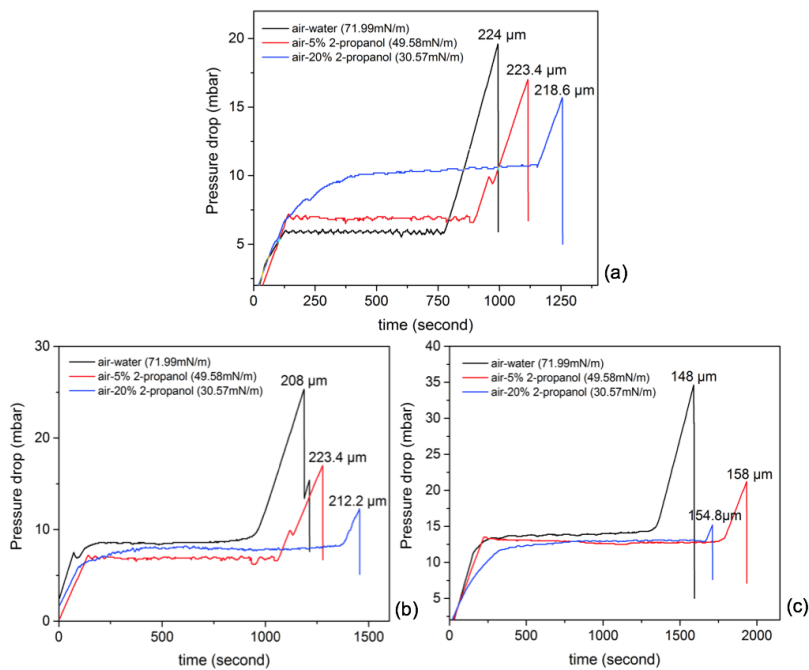
pore throat.

Fig. 9 Effect of liquid surface tension and capillary tip diameter on the pressure-

drop profiles of two-phase flow in constricted capillaries (The surface tensions:

air-water = 71.99 mN/m, air-5%wt 2-propanol = 49.58 mN/m and air-20%wt 2-

propanol = 30.57 mN/m)

In Fig. 9, the peak of the pressure drop for air-water flows is largest among

three types of two-phase flows, as the surface tension of air-water is highest.

According to the Young-Laplace equation ($\Delta P_c \propto \gamma$), the two-phase interface

with a larger surface tension will induce a higher capillary resistance. This can explain the difference in pressure profiles measured for gas-liquid interface with different surface tension, only when the pore size is smaller than the effective pore throat. However, it cannot explain why the impact of surface tension on the resistant pressure suddenly starts from the critical point-the effective pore throat. In Section 4-6, the sudden increase in capillary resistance is qualitatively explained through pore contact angle.
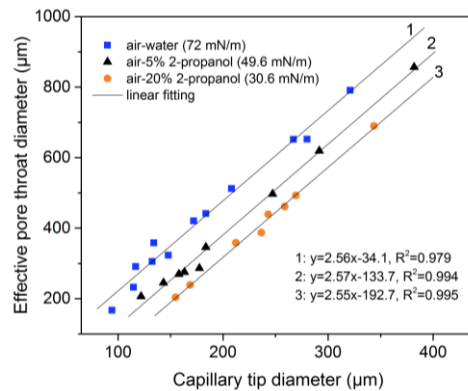

Fig. 10 Impact of surface tension on the effective pore throat

The three fitted lines in Fig. 10 indicate that fluid surface tension affects the effective pore throat diameter of constricted capillaries for two-phase flows. For the gas-liquid flows with a smaller surface tension, the effective pore throat diameter in the microchannel would be smaller. For example, in a capillary with tip diameter of 200 μm, the effective pore throat is the highest for air-water flow (around 480 μm, as shown in Fig. 10,) because of the highest surface tension

of air-water interface (71.99 mN/m). On the contrary, the effective pore throat diameter for air-20%wt 2-propanol interface is the smallest (about 300 μm) among the three cases, as it has the lowest surface tension (39.57 mN/m). It is interesting to note that the gradients of three fitted lines are nearly the same. During the experiments, viscosity of DI water, 5%wt 2-propanol and 20%wt 2-propanol, and the capillary geometry were very similar, and the gas volume and liquid flowrate were the same. The same gradient of the lines in Fig. 10 means that the impact of the capillary tip size on the diameter of effective pore throat is the same even though the air-liquid interfaces have various surface tensions.

4.4 Effect of liquid viscosity on the effective pore throat

The effect of viscosity on the effective pore throat was investigated through injecting silicone oil with viscosities from 10 to 500 cst to create a silicone oil-water flow in constricted capillaries. The physical properties of different silicone oils are presented in Table 4. The experimental results are presented in Figs. 11-12. The results indicate that viscosity significantly affects the magnitude of the pressure drop in fluids flows (Fig. 11), but does not affect the diameter of the effective pore throat (Fig. 12). The resistant pressure drop of silicone oil flow in constricted capillaries increases with fluids viscosity. When the viscosity increases from 10 to 100 cst, the pressure drop for the silicone oil in a constricted capillary with a tip diameter of 339 μm increases from 5 to 35 mbar.

> **Commented [CC2]:**
>
> **Commented [FX3]:** If there is no problem, do not change it.
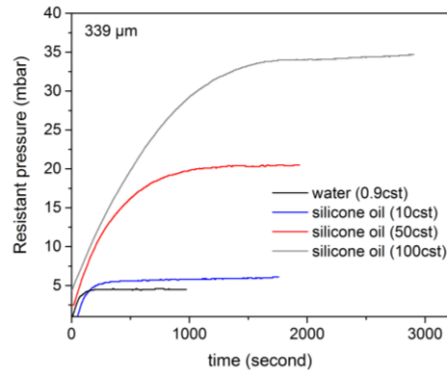> To avoid more problems from the reviewer.

Fig. 11 Effect of viscosity on the pressure drop for silicone oil flows in a constricted capillary with a tip diameter of 339 μm

Fig. 12 shows the effect of viscosity (from 10 to 500 cst) on the effective pore throat for silicone oil-water flows in constricted capillaries. The diameter of effective pore throat is similar even the viscosity of silicone oil varies significantly from 10 to 500 cst. The data indicates that the effective pore throat diameter is independent of fluid viscosity. Viscosity can affect the magnitude of resistance to phase body, but does not affect the resistance to the two-phase interface. A larger fluid viscosity will result in a higher frictional pressure drop, which is easily explained by Hagen-poiseuille equation, thus the resistance to fluid body is greater. As the resistance to the interface is induced by the surface tension, rather than viscosities, viscosity does not influence the diameter of effective pore throat.
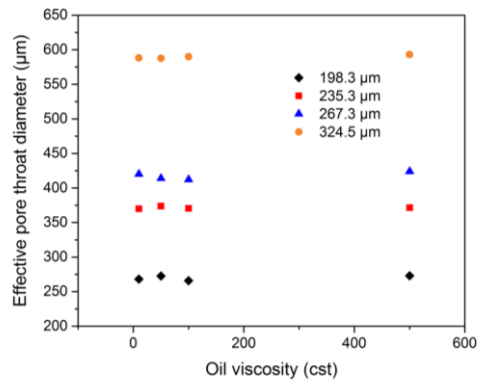
Commented [CC4]:

Fig. 12 Effect of viscosity on effective pore throat for silicone oil-water interfaces with different viscosities

4.5 Impact of capillary geometry on the effective pore throat

Capillary geometry in this study includes the capillary length, capillary gradient and capillary tip diameter. Figs. 8 and 10 show that, within a certain range, the effective pore throat diameter linearly increases with the capillary tip diameter. For liquids with various surface tension, a large capillary tip diameter gives a large effective pore throat. As the capillary length is fixed in this study, the gradient of the capillary tapered section can be simply calculated by dividing the diameter difference at the two end of the capillary by the length. Fig. 13 illustrates the impact of capillary gradient on the diameter of effective pore throat diameter. Effective pore throat diameter almost linearly increases with the capillary gradient. Interestingly, the pressure increase rate does not show any obvious dependence on the capillary tip diameter or the capillary gradient. As shown in Figs. 4-6, the pressure increase sections in the pressure profiles

have a similar increase rate for all gas-liquid flows in the capillaries with diameters in a wide range from 94 to 291.6 μm.
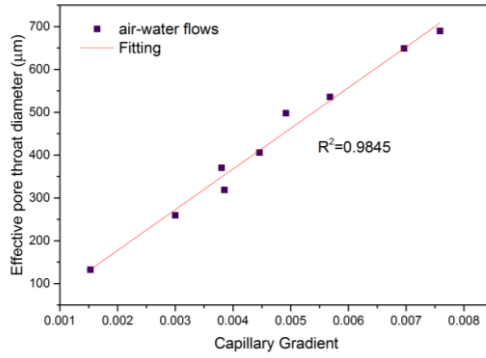

Fig. 13 Impact of capillary gradient on the effective pore throat

4.6 Discussions

As discussed in 4.1, the resistance increase is attributed to the capillary force induced by the bubble phase, while no theory explained this sudden increase in resistant pressure as well as the effective pore throat. According to 'Jamin' effect and literature [60], the capillary pressure resulting from the motion of bubble in constricted microchannel equals the difference of capillary pressure between two sides of the bubble, as shown in Fig. 2 (b), and it is calculated through equation (11).

$$\Delta P_c = P_B - P_A = \frac{2\gamma cos\theta_a}{r_a} - \frac{2\gamma cos\theta_b}{r_b} \tag{11}$$
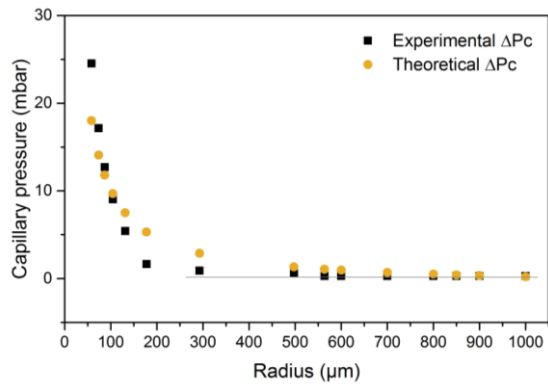
Fig. 14 A plot of the change of capillary pressure with the flow path radius for air-water flow in the constricted capillary with the tip size of 94 µm

Fig. 14 compares the experimental capillary pressure and the theoretical capillary pressure for air-water flows in a constricted capillary, and it indicates that the capillary pressure calculated through equation (11) is smoothly and continuously changed with flow path radius under the condition that the contact angle and the surface tension are fixed. However, the experimental capillary pressure is not smoothly changed with flow radius (as shown in Figs. 15-16), and the effective pore throat separates the capillary pressure profile into two straight lines with different gradients. When the channel pore size is greater than the effective pore throat, capillary pressure does not vary with the pore size. After the effective pore throat, capillary pressure suddenly increases with the decrease of pore size. The theoretical equations cannot indicate the size of effective pore throat and capillary pressure drop of fluid interface in constricted capillaries within a large range of pore size.
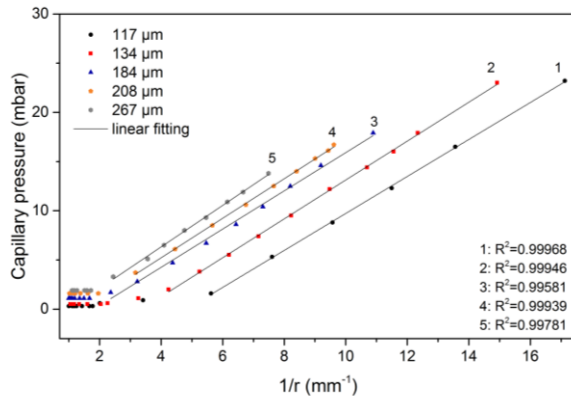
Fig. 15 ΔP_c vs. *1/r* for air-water flows in constricted capillaries with different tip diameters

However, the effective pore throat and the sudden increase in the resistant pressure profiles could be qualitatively explained by the pore contact angle published by our group [61, 62]. Contact angle measured from a pore space differs significantly from that on a flat surface. For a certain vapor-liquid interface and solid surface, the static contact angle on a flat surface is a constant. In a pore space, the static pore contact angle for air-water interface increases with the decrease of pore size until around 200-400 μm, and then takes a constant value of around 33 degrees (as shown in Fig. 16) [61]. When the pore size is greater than the effective pore throat, with the decrease of pore size, the pore contact angle increases, i.e. *cosθ* decreases. The capillary pressure may remain constant in this section due to the decrease of *cosθ* and the decrease of *r* at the same time. Once the pore size is smaller than the

effective pore throat, the pore contact angle is roughly a constant. The capillary pressure therefore linearly increases with *1/r*. The turning point in the contact angle profile roughly matches the effective pore throat.
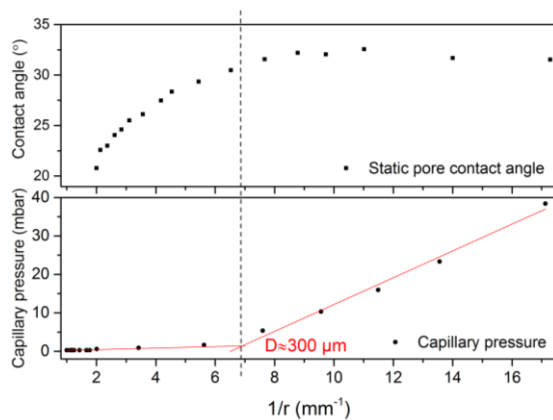

Fig. 16 Change of static pore contact angle with *1/r*, and change of capillary pressure with *1/r* for the air-water flows in the constricted capillary with a tip size of 117 μm

From the aspect of the interfacial free energy, pore contact angle can also explain the measured pressure profile and the effective pore throat. For an isothermal, closed system, the interfacial free energy (dF) can be calculated through equation (12) [1], [63],

$$dF = \gamma_{sg}dA - \gamma_{sl}dA - \gamma_{lg}dA \; cos\theta \tag{12}$$

Where γ is the interfacial tension for the liquid-gas (*lg*), solid-gas (*sg*) and solid-liquid (*sl*) interfaces, dA is the moving area of interface and θ is the equilibrium contact angle among the three-phase.

When the pore size is larger than the effective pore throat, the pore contact angle increases with the decrease of pore size, i.e. $cos\theta$ is decreasing. The interfacial free energy (dF) increases correspondingly, which means more energy is stored in the interface, therefore the energy dissipation which is reflected through pressure drop is not significant. This corresponds to the horizontal section of capillary pressure profile. When the channel pore size is smaller than the effective pore throat, the contact angle does not vary with pore size, and the two-phase interface cannot store extra energy, therefore the capillary pressure drop (ΔP_c) starts to increase sharply with the decrease of pore size.

Conclusions

The paper investigates the effective pore throat of a micro-channel with varied diameter and the effect of the surface tension, pore contact angle (not flat surface contact angles), viscosity and tip diameter of constricted capillaries on the effective pore throat. The pressure drops were measured to evaluate the resistance to two-phase interface in constricted capillaries and to identify the effective pore throat. "Effective pore throat" is defined to determine at what pore size the capillary resistance starts to apply to two-phase interfaces in a microchannel with varied pore size.

The size of effective pore throat depends on liquid surface tension and capillary geometry (capillary tip diameter and capillary gradient). The higher the

interfacial tension of gas-liquid interfaces, the larger the diameter of the effective pore throat. The capillary with a smaller tip diameter, or a smaller gradient will give a smaller effective pore throat diameter. Fluid viscosity only affects the magnitude of the resistance to fluids flows in microchannels, but not affect the diameter of the effective pore throat.

Surface tension affects the resistance to the two-phase flows only when the channel has a size smaller than the effective pore throat. The larger the surface tension, the greater the resistant pressure to two-phase interfaces. For channels with pore size greater than the effective pore throat, the resistant pressure drop depends on capillary tip diameter, rather than the surface tension. The sudden change in the resistant pressure profile, and the effective pore throat cannot be explained by the contact angle on a flat surface, but it could be explained by the pore contact angle. The difference in the capillary pressure profile before and after the effective pore throat matches the change in the pore contact angle with the pore size.

Reference

[1] N.R. Morrow, Physics and Thermodynamics of Capillary Action in Porous Media, J. Ind. Eng. Chem. 62 (1970) 32-56.
[2] P.S. Ringrose, K.S. Sorbie, P.W.M. Corbett, J.L. Jensen, Immiscible flow behaviour in laminated and cross-bedded sandstones, J. Pet. Sci. Eng. 9 (1993) 103-124.
[3] P. Quan, M.C. Lai, Numerical study of water management in the air flow channel of a PEM fuel cell cathode, J. Power Sources 164 (2007) 222-237.
[4] P.K. Sinha, P.P. Mukherjee, C.Y. Wang, Impact of GDL structure and wettability on water management in polymer electrolyte fuel cells, J.

Mater. Chem. 17 (2007) 3089-3103.

[5] A. Tanimu, S. Jaenicke, K. Alhooshani, Heterogeneous catalysis in continuous flow microreactors: A review of methods and applications, Chem. Eng. J. 327 (2017) 792-821.

[6] Z. Lian, K. Jae-Mo, J. Linan, M. Asheghi, K.E. Goodson, J.G. Santiago, T.W. Kenny, Measurements and modeling of two-phase flow in microchannels with nearly constant heat flux boundary conditions, J. Microelectromech. Syst. 11 (2002) 12-19.

[7] M. Sharan, A.S. Popel, A two-phase model for flow of blood in narrow tubes with increased effective viscosity near the wall, Biorheology 38 (2001) 415-428.

[8] R. Parmar, S.K. Majumder, Microbubble generation and microbubble-aided transport process intensification-A state-of-the-art report, Chem. Eng. Process. 64 (2013) 79-97.

[9] H.K. Sarma, B.B. Maini, K. Jha, Evaluation of emulsified solvent flooding for heavy oil recovery, J. Can. Pet. Technol. 37 (1998) 55-62.

[10] T. Ramstad, N. Idowu, C. Nardi, P.E. Oren, Relative Permeability Calculations from Two-Phase Flow Simulations Directly on Digital Images of Porous Rocks, Transport Porous Med. 94 (2012) 487-504.

[11] P.C. Reeves, M.A. Celia, A functional relationship between capillary pressure, saturation, and interfacial area as revealed by a pore-scale network model, Water Resour. Res. 32 (1996) 2345-2358.

[12] C. Choi, D.I. Yu, M. Kim, Surface wettability effect on flow pattern and pressure drop in adiabatic two-phase flows in rectangular microchannels with T-junction mixer, Exp. Therm. Fluid Sci. 35 (2011) 1086-1096.

[13] S. Lin, C.C.K. Kwok, R.Y. Li, Z.H. Chen, Z.Y. Chen, Local Frictional Pressure-Drop during Vaporization of R-12 through Capillary Tubes, Int. J. Multiph. Flow 17 (1991) 95-102.

[14] C.Y. Lee, S.Y. Lee, Pressure drop of two-phase plug flow in round mini-channels: Influence of surface wettability, Exp. Therm. Fluid Sci. 32 (2008) 1716-1722.

[15] N.C. Wardlaw, The Effects of Geometry, Wettability, Viscosity and Interfacial-Tension on Trapping in Single Pore Throat Pairs, J. Can. Pet. Technol. 21 (1982) 21-27.

[16] M.C. Liang, Y.M. Liu, B.Q. Xiao, S.S. Yang, Z.K. Wang, H.M. Han, An analytical model for the transverse permeability of gas diffusion layer with electrical double layer effects in proton exchange membrane fuel cells, Int. J. Hydrog. Energy 43 (2018) 17880-17888.

[17] P.M.Y. Chung, M. Kawaji, The effect of channel diameter on adiabatic two-phase flow characteristics in microchannels, Int. J. Multiph. Flow 30 (2004) 735-761.

[18] S. Saisorn, S. Wongwises, The effects of channel diameter on flow

pattern, void fraction and pressure drop of two-phase air-water flow in circular micro-channels, Exp. Therm. Fluid Sci. 34 (2010) 454–462.

[19] J. Yue, G.W. Chen, Q. Yuan, Pressure drops of single and two-phase flows through T-type microchannel mixers, Chem. Eng. J. 102 (2004) 11–24.

[20] M.C. Liang, S.S. Yang, T.J. Miao, B.M. Yu, Minimum applied pressure for a drop through an abruptly constricted capillary, Microfluid. Nanofluid. 19 (2015) 1–8.

[21] M. Andrew, B. Bijeljic, M.J. Blunt, Pore-scale imaging of trapped supercritical carbon dioxide in sandstones and carbonates, Int. J. Greenh. Gas Control 22 (2014) 1–14.

[22] W.L. Olbricht, Pore-scale prototypes of multiphase flow in porous media, Annu. Rev. Fluid Mech. 28 (1996) 187–213.

[23] M. Sahimi, Characterization of Pore Space Connectivity: Percolation Theory, Flow and Transport in Porous Media and Fractured Rock, Wiley-VCH Verlag GmbH & Co. KGaA2011, pp. 15–37.

[24] M.J. Blunt, Flow in porous media – pore-network models and multiphase flow, Curr. Opin. Colloid Interface Sci. 6 (2001) 197–207.

[25] P.H. Nelson, Pore-throat sizes in sandstones, tight sandstones, and shales, AAPG Bull. 93 (2009) 329–340.

[26] C.N. Zou, R.K. Zhu, K.Y. Liu, L. Su, B. Bai, X.X. Zhang, X.J. Yuan, J. Wang, Tight gas sandstone reservoirs in China: characteristics and recognition criteria, J. Pet. Sci. Eng. 88–89 (2012) 82–91.

[27] W.B. Lindquist, A. Venkatarangan, J. Dunsmuir, T.F. Wong, Pore and throat size distributions measured from synchrotron X-ray tomographic images of Fontainebleau sandstones, J. Geophys. Res-Solid Earth 105 (2000) 21509–21527.

[28] H. Dong, M.J. Blunt, Pore-network extraction from micro-computerized-tomography images, Phys. Rev. E. 80 (2009) 036307.

[29] Z. Liu, Y. Yang, J. Yao, Q. Zhang, J. Ma, Q. Qian, Pore-scale remaining oil distribution under different pore volume water injection based on CT technology, Adv. Geo-Energ. Res. 1 (2017) 171–181.

[30] B.S. Nabawy, Y. Geraud, P. Rochette, N. Bur, Pore-throat characterization in highly porous and permeable sandstones, AAPG Bull. 93 (2009) 719–739.

[31] C.D. Tsakiroglou, A.C. Payatakes, Characterization of the pore structure of reservoir rocks with the aid of serial sectioning analysis, mercury porosimetry and network simulation, Adv. Water Resour. 23 (2000) 773–789.

[32] A. Golparvar, Y. Zhou, K.J. Wu, J.S. Ma, Z.X. Yu, A comprehensive review of pore scale modeling methodologies for multiphase flow in porous media, Adv. Geo-Energy Res. 2 (2018) 418–440.

[33] P.-E. Øren, S. Bakke, Reconstruction of Berea sandstone and pore-scale modelling of wettability effects, J. Pet. Sci. Eng. 39 (2003)

177-199.

[34] J.F. Roca, M.S. Carvalho, Flow of a drop through a constricted microcapillary, Comput. Fluids 87 (2013) 50-56.

[35] S. Cobos, M.S. Carvalho, V. Alvarado, Flow of oil-water emulsions through a constricted capillary, Int. J. Multiph. Flow 35 (2009) 507-515.

[36] T. Metz, N. Paust, R. Zengerle, P. Koltay, Capillary driven movement of gas bubbles in tapered structures, Microfluid. Nanofluid. 9 (2010) 341-355.

[37] S. Roman, M.O. Abu-Al-Saud, T. Tokunaga, J. Wan, A.R. Kovscek, H.A. Tchelepi, Measurements and simulation of liquid films during drainage displacements and snap-off in constricted capillary tubes, J. Colloid Interface Sci. 507 (2017) 279-289.

[38] C. Chao, X. Xu, S.O. Kwelle, X. Fan, Significance of gas-liquid interfaces for two-phase flows in micro-channels, Chem. Eng. Sci. 192 (2018) 114-125.

[39] W.R. Rossen, P.A. Gauglitz, Percolation Theory of Creation and Mobilization of Foams in Porous-Media, AICHE J. 36 (1990) 1176-1188.

[40] C.D. Mcauliffe, Oil-in-Water Emulsions and Their Flow Properties in Porous Media, J. Petrol. Technol. 25 (1973) 727-733.

[41] S. Peng, Q.H. Hu, S. Dultz, M. Zhang, Using X-ray computed tomography in pore structure characterization for a Berea sandstone: Resolution effect, J. Hydrol. 472 (2012) 254-261.

[42] M.J.F. Warnier, M.H.J.M. de Croon, E.V. Rebrov, J.C. Schouten, Pressure drop of gas–liquid Taylor flow in round micro-capillaries for low to intermediate Reynolds numbers, Microfluid. Nanofluid. 8 (2009) 33-45.

[43] M.T. Kreutzer, F. Kapteijn, J.A. Moulijn, C.R. Kleijn, J.J. Heiszwolf, Inertial and interfacial effects on pressure drop of Taylor flow in capillaries, AICHE J. 51 (2005) 2428-2440.

[44] F.P. Bretherton, The Motion of Long Bubbles in Tubes, J. Fluid Mech. 10 (1961) 166-188.

[45] E.W. Washburn, The dynamics of capillary flow., Phys. Rev. 17 (1921) 273-283.

[46] F.A.L. Dullien, Porous Media Fluid transport and pore structure Academic Press, San Diego, 1992.

[47] H. Cho, H.Y. Kim, J.Y. Kang, T.S. Kim, How the capillary burst microvalve works, J. Colloid Interface Sci. 306 (2007) 379-385.

[48] N. Ichikawa, K. Hosokawa, R. Maeda, Interface motion of capillary-driven flow in rectangular microchannel, J. Colloid Interface Sci. 280 (2004) 155-164.

[49] A. Hebach, A. Oberhof, N. Dahmen, A. Kogel, H. Ederer, E. Dinjus, Interfacial tension at elevated pressures – Measurements and correlations in the water plus carbon dioxide system, J. Chem. Eng.

Data 47 (2002) 1540-1546.

[50] E.W. Hough, M.J. Rzasa, B.B. Wood, Interfacial Tensions at Reservoir Pressures and Temperatures - Apparatus and the Water-Methane System, Pet. Trans. AIME 192 (1951) 57-60.

[51] H.Y. Jennings Jr, G.H. Newman, The effect of temperature and pressure on the interfacial tension of water against methane-normal decane mixtures, Soc. Pet. Eng. J 11 (1971) 171-175.

[52] F.M. Pang, C.E. Seng, T.T. Teng, M.H. Ibrahim, Densities and viscosities of aqueous solutions of 1-propanol and 2-propanol at temperatures from 293.15 K to 333.15 K, J. Mol. Liq. 136 (2007) 71-78.

[53] G. Vazquez, E. Alvarez, J.M. Navaza, Surface-Tension of Alcohol Plus Water from 20-Degrees-C to 50-Degrees-C, J. Chem. Eng. Data 40 (1995) 611-614.

[54] W.K. Chan, C. Yang, Surface-tension-driven liquid-liquid displacement in a capillary, J. Micromech. Microeng. 15 (2005) 1722-1728.

[55] G.G. Giordano, M.F. Refojo, Silicone oils as vitreous substitutes, Prog. Polym. Sci. 23 (1998) 509-532.

[56] J.W. Peterson, J.C. Berg, Surface Fractionation of Multicomponent Oil Mixtures, Ind. Eng. Chem. Fund. 25 (1986) 668-677.

[57] W.O. Smith, M.D. Crane, The Jamin effect in cylindrical tubes, J. Am. Chem. Soc. 52 (1930) 1345-1349.

[58] M.J. Martinez, K.S. Udell, Axisymmetric Creeping Motion of Drops through Circular Tubes, J. Fluid Mech. 210 (1990) 565-591.

[59] R. Wright, Jamin effect in oil production, AAPG Bull. 17 (1933) 1521-1526.

[60] D.W. Green, G.P. Willhite, Enhanced oil recovery, Henry L. Doherty Memorial Fund of AIME, Society of Petroleum Engineers Richardson, TX1998.

[61] X.X. Li, X.F. Fan, S. Brandani, Difference in pore contact angle and the contact angle measured on a flat surface and in an open space, Chem. Eng. Sci. 117 (2014) 137-145.

[62] X.X. Li, X.F. Fan, A. Askounis, K.J. Wu, K. Sefiane, V. Koutsos, An experimental study on dynamic pore wettability, Chem. Eng. Sci. 104 (2013) 988-997.

[63] J.D. Andrade, L.M. Smith, D.E. Gregonis, The Contact Angle and Interface Energetics, in: J.D. Andrade (Ed.) Surface and Interfacial Aspects of Biomedical Polymers: Volume 1 Surface Chemistry and Physics, Springer US, Boston, MA, 1985, pp. 249-292.